*29th EPS Conference on Plasma Phys. and Contr. Fusion Montreux, 17-21 June 2002 ECA Vol. **26B**, P-4.057 (2002)*

Physics of Off-Axis Electron Cyclotron Current Drive

R. Prater,[1] C.C. Petty,[1] R. Harvey,[2] Y.-R. Lin-Liu,[3] J.M. Lohr,[1] T.C. Luce[1]

[1]*General Atomics, P.O. Box 85608, San Diego, California 92186-5608 USA*
[2]*CompX, P.O. Box 2672, Del Mar, California 92014-5672 USA*
[3]*Department of Physics, National Dong Hwa University, Hualien, Taiwan*

ABSTRACT: Electron cyclotron current drive is a key option for driving current off-axis in a tokamak, as needed for example for current profile control or for suppression of neoclassical tearing modes. Experiments in DIII–D at low beta have shown that the partial cancellation of the Fisch-Boozer co-current by the Ohkawa counter-current can cause strong deterioration of the current drive efficiency at larger minor radius. However, more recent experiments at higher power have shown that the loss in efficiency can be mostly recovered if the target plasma has higher electron beta, β_e. The improvement in efficiency with beta can be understood from a theoretical viewpoint by applying the Fokker-Planck code CQL3D, which shows excellent agreement with experiment over a wide range of parameters, thereby validating the code as an effective means of predicting the ECCD.

Electron cyclotron current drive (ECCD) is a key element of the advanced tokamak program on DIII–D, the goal of which is to develop high performance discharges with the potential for economical steady-state operation. Extensive computational modeling has shown that ECCD is an excellent tool for sustaining the current profile which supports improved confinement and stability as well as for stabilizing MHD activity like neoclassical tearing modes. Validation of the models used in the calculations is needed to support these applications of ECCD.

Measurements of plasma current driven by ECCD have been made over a very broad range of parameters, including electron density and temperature, normalized minor radius ρ between 0.1 and 0.4, poloidal location on a flux surface, parallel index of refraction $n_{||}$ between –0.5 and 0.5, and plasma edge conditions (L–mode and H–mode). The driven current is obtained from an analysis of the magnetic pitch angles near the plasma midplane determined from motional Stark effect measurements [1]. For each experimental case the driven current can be calculated by the linear TORAY-GA code and the quasilinear Fokker-Planck code CQL3D [2]. The Fokker-Planck code results are expected to be more accurate since the effects of the parallel dc electric field are taken into account including the effect of quasilinear modification to the resistivity and the collision model is more accurate (i.e., momentum is conserved in electron-electron collisions and the high-velocity approximation to the collision operator is not made as in the linear codes [3]).

These measurements are summarized in Fig. 1 [4], in which the measured current is shown to be in excellent agreement with the Fokker-Planck code calculations for the complete data set, including discharges with negative $n_{||}$ corresponding to counter-current drive. This agreement strongly validates the CQL3D code over the range of experimental parameters. The agreement between the TORAY-GA calculations of the driven current and experiment is not quite as good [4], particularly for the cases with larger driven current in which quasilinear effects might be expected , but for many cases and purposes the agreement is also adequate.

It is expected from theory that trapping of the current-carrying electrons in the magnetic well will lead to reduced current drive efficiency. Data from Fig. 1 may be selected and replotted to illustrate the physics of the effects of trapping on ECCD. The normalized current drive efficiency [5] $\zeta = (e^3/e_0^2)\, I_{EC} n_e R/P_{EC} T_e$ is plotted in Fig. 2 for measurements of ζ for current drive at a fixed location (ρ of 0.3 and 0.4, poloidal angle near 90°) as a function of the

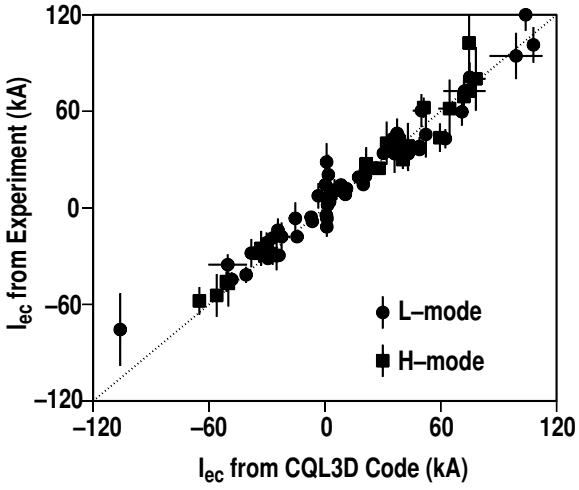

Fig. 1. The measured current driven by ECCD versus the current calculated by the CQL3D Fokker-Planck code for the experimental conditions [4]. The dotted line represents perfect agreement.

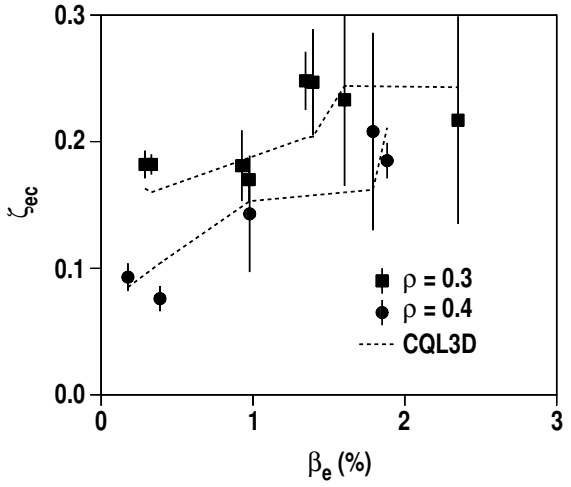

Fig. 2. The measured normalized current drive efficiency as a function of β_e, for ρ=0.3 (squares) and ρ=0.4 (circles) [4]. In all cases the poloidal angle is near 90°. The dotted lines represent the results of calculations for the experimental conditions.

local electron beta β_e. These plots show that the current drive efficiency increases strongly with β_e, especially at the larger ρ where trapping effects should be larger. At the highest β_e the normalized efficiency at ρ=0.4 is almost the same as that at ρ=0.3. Figure 2 also shows the results of calculations of ζ from the CQL3D code, which are highly consistent with the measurements. These results are very favorable for applications such as those mentioned above which require that the current be driven at a normalized minor radius of 0.5 to 0.8 where the magnetic well depth is large. At present measurements of current drive at ρ greater than 0.4 have not been made, although suppression of neoclassical tearing modes by ECCD [6] has indicated that the efficiency at ρ=0.6 should be close to the theoretical efficiency.

The strong recovery of the efficiency of off-axis current drive with β_e can be understood by considering the effects of increasing density and temperature on the wave absorption and the resulting electron diffusion in velocity space. The electron cyclotron resonance written for low-field-side launch of waves near the second harmonic is

$$\omega = 2\Omega_0/\gamma + k_{||}\, v_{||} \quad , \tag{1}$$

where ω is the applied frequency, Ω_0=eB/m is the nonrelativistic cyclotron frequency, γ is the relativistic factor, $k_{||}$ is the applied wavenumber, and $v_{||}$ is the parallel velocity of a resonant electron. Defining $y=(\omega/2\Omega_0)^2$ and $n_{||}=ck_{||}/\omega$, this becomes

$$\frac{v_\perp^2}{v_t^2} = \frac{1-y}{v_t^2}c^2 + \left[\frac{2n_{||}yc}{v_t}\right]\frac{v_{||}}{v_t} - \left(1+n_{||}^2 y\right)\frac{v_{||}^2}{v_t^2} \quad , \tag{2}$$

where $v_t = c[(T_* + T_*^2/4)/(1 + T_* + T_*^2/4)]^{1/2}$ is the thermal velocity and $T_*=kT_e/mc^2$ is the electron temperature normalized to the rest mass energy. In this equation the velocities have been normalized by v_t in order to connect heuristically to the wave-particle interaction which occurs typically at 1 to 3 times the thermal velocity.

For the purposes of this study the key is to evaluate Eq. (2) at the physical location in the plasma where the wave power is absorbed at the maximum rate per unit ray length. This is done for a fixed set of conditions, namely the equilibrium, the kinetic profiles [T_e(ρ),

$n_e(\rho)$, $Z_{eff}(\rho)$], and the EC ray launching angles. Note that this location is not the maximum of the absorption coefficient along the ray path, since the ray may be well attenuated before reaching that location. The ray tracing code TORAY-GA is used to determine the coordinates (R,z) of the maximum attenuation rate, and the local T_e, $n_{||}$, and B then fully determine the resonance curve for that location.

This computational process has been applied to the conditions of a discharge with the EC wave launched so as to intersect the resonance directly above the magnetic axis (poloidal angle 90°) at a normalized minor radius of 0.4. The resonance curve is shown in Fig. 3. Also drawn is the trapped-passing boundary, which is simply a straight line through the origin at an angle $\text{asin}[(B_{local}/B_{max})^{1/2}]$ from the vertical axis, with electrons above the boundary trapped. The resonance clearly lies in the vicinity of the trapped region and the wave-particle interaction with the boundary may be expected.

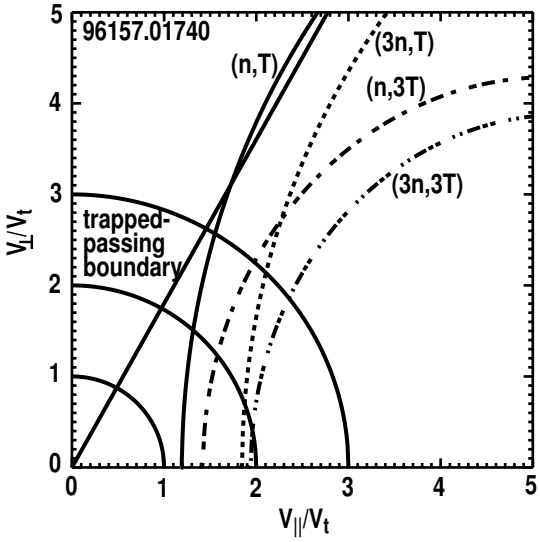

Fig. 3. The electron cyclotron resonance curve plotted as a function of $v_\perp/v_t$ and $v_{||}/v_t$ for the experimental conditions (solid curve, n_e = 1.57×10^{19} m^{-3}, T_e=1.29 keV, $n_{||}$=0.518) and for other conditions (dashed curve: 3 times higher n_e; dotted curve, 3 times higher T_e; and chain dash, both n_e and T_e 3 times higher). Also shown is the trapped-passing boundary for the mirror ratio 1.23. The plasma is an L-mode discharge in DIII–D with low local electron beta of 0.14%, and the peak of wave attenuation is at ρ=0.385 and poloidal angle near 90°.

The temperature and density in the calculation may be arbitrarily changed to illustrate their effects on the resonance. For example, Fig. 3 shows three other cases. In these other cases, the ray launching angles in the calculation were changed slightly or the toroidal magnetic field was adjusted by up to 5% to keep the location of the maximum absorption rate and the $n_{||}$ there constant for all cases. First, n_e was increased by a factor 3. Because there are more electrons the wave absorption coefficient is larger, so the location of maximum attenuation moves further from the cold resonance, requiring a larger Doppler shift in Eq. (1). This shows up as a shift in the resonance curve in Fig. 3 to the right, away from the trapping boundary even though Eq. (2) has no explicit dependence on density. Alternatively, T_e was increased by a factor 3. Since higher T_e also increases absorption this also shifts the resonance curve to the right. Raising T_e has the additional effect of curving the resonance away from the trapping boundary due to the explicit $T*$ dependence in Eq. (2). Finally, increasing both n_e and T_e by a factor 3 shifts the curve and bends it more strongly away from the trapping boundary.

It is this effect of increased density and/or temperature on the location of the resonance relative to the trapping boundary which accounts for the improvement in the efficiency of off-axis ECCD in plasmas with higher β_e. In describing the physics of this effect, the proper dimensionless physical quantities are $T*$ from Eq. (2) and ω_p^2/Ω_0^2 (which is proportional to n_e) from the absorption coefficient for the second harmonic X-mode [7], where ω_p is the plasma frequency. Since both dimensionless variables tend to reduce the effect of trapping, their product β_e may be a suitable shorthand roughly describing their combined effect.

It should be noted that this behavior is valid for the fundamental O-mode as well as the second harmonic X-mode but not valid for the fundamental X-mode for which the absorption coefficient is inversely proportional to density. Another geometric factor which can affect ζ by moving the absorption location away from the trapping boundary is the angle of incidence

of the ray, given by (B/R)/(dB/ds), where s is the arc length along the ray. In this work this variable does not change much and is neglected, but in experiments where the rays are launched nearly parallel to the axis of symmetry this factor can be very important.

Any electron satisfying Eq. (2) is resonant with the wave. However, not all resonant electrons interact strongly with the wave. For example, absorption of the second harmonic X-mode is a finite Larmor radius effect, so electrons with small $v_\perp$ interact only weakly with the wave. In order to see more clearly the electrons which are affected by the wave, the CQL3D code was applied to these model cases. CQL3D calculates a solution to the relativistic bounce-averaged Fokker-Planck code including a source term representing the diffusion induced by the rf waves. This code calculates the distribution function and other quantities fully relativistically, as a function of parallel and perpendicular momentum per unit rest mass normalized to an arbitrary maximum energy; in this work, these coordinates have been translated to the particle velocity normalized by the thermal velocity as defined in Eq. (2).

The CQL3D calculations for model cases clearly show the effect on the normalized efficiency of increasing n_e and T_e. Figure 4 shows two cases for geometry similar to that of Fig. 3, one with low β_e ($n_e(0) = 2\times10^{19}$ m^{-3}, T_e=4 keV) and one with 9 times higher β_e ($n_e(0)=6\times10^{19}$ m^{-3}, T_e=12 keV). Figure 4 shows the particle flux in velocity space due to rf diffusion at the location of maximum rate of ray attenuation. In the low β_e case the wave-induced flux causes strong interaction with the trapping boundary, while in the high β_e case the wave interaction is far from the trapping boundary. This illustrates the process by which the trapping effect is mitigated at high β_e.

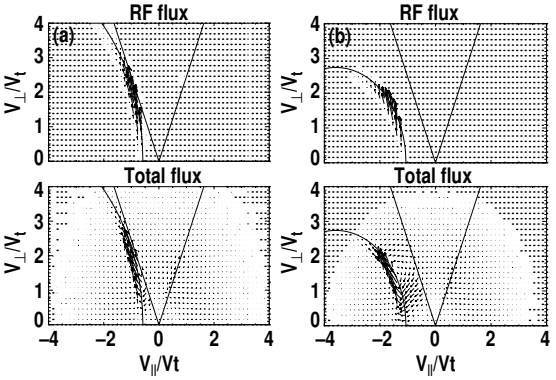

Fig. 4. The flux in velocity space due to the wave-particle interaction (upper panels) and the total flux including collisional effects (lower panels) calculated by CQL3D for two cases: (a) low β_e ($n_{e0}=2\times10^{19}$ m^{-3}, T_{e0}=4 keV) and (b) higher β_e ($n_{e0}=6\times10^{19}$ m^{-3}, T_{e0}=12 keV). In both cases ρ=0.385 and poloidal angle is near 90°.

Work supported by U.S. Department of Energy under Contract DE-AC03-99ER54463 and Grant DE-FG03-99ER54541.

REFERENCES

[1] C.C. Petty, et al., Nucl. Fusion **41**, (2001) 551.

[2] R.W. Harvey and M. McCoy, Proc. IAEA Tech.Comm. Mtg. On Adv. In Simulation and Modeling of Thermonuclear Plasmas, Montreal, Canada, 1992 (IAEA, Vienna, 1993), p. 489.

[3] Ronald H. Cohen, Phys. Fluids **30**, (1987) 2442.

[4] C.C. Petty, et al., "Detailed measurements of the electron cyclotron current drive efficiency on DIII-D," General Atomics Report GA-A23949 (2002); submitted for publication in Nucl. Fusion.

[5] T.C. Luce, et al., Phys. Rev. Letters **83**, (1999) 4550.

[6] R. Prater, et al., in Fusion Energy 2000, 18th Conference Proceedings, Sorrento, Italy 2000 (IAEA, 2001), paper EX8/1.

[7] M. Bornatici, et al., Nucl. Fusion **23**, (1983) 1153.